Tellus (1997), 49B, 231–248
Printed in UK – all rights reserved

TELLUS
ISSN 0280–6509

Semi-Lagrangian modelling of tropospheric ozone

By JANUSZ A. PUDYKIEWICZ[1] and A. KALLAUR, *Atmospheric Environment Service, Dorval, Québec, Canada H9P 1J3,* and PIOTR K. SMOLARKIEWICZ, *National Center for Atmospheric Research*, Boulder, Colorado 80307, USA*

(Manuscript received 11 March 1996; in final form 7 November 1996)

ABSTRACT

The occurrence of high concentrations of ozone in the lower part of the troposphere is considered as one of the most important issues of tropospheric chemistry. The chemical mechanisms of tropospheric ozone formation are complex, and highly variable meteorological conditions contribute additionally to difficulties in an accurate prediction of ozone episodes. An effective way to increase our understanding of the problem and eventually improve our ability to predict the concentration of tropospheric ozone and to formulate emission control strategies is by applying a comprehensive model representing accurately the interaction between meteorological processes and chemical reactions. This paper presents a 3-dimensional semi-Lagrangian, chemical tracer model (CTM) featuring an accurate transport algorithm, comprehensive oxidants chemistry and deposition modules. The CTM is executed in off–line mode with a semi-Lagrangian, nonhydrostatic, mesoscale meteorological model that contains an extensive parameterization of physical processes (including a boundary layer scheme and clouds). The system of models was run for a time period of 6 days in order to generate a tropospheric ozone field during a smog episode observed in the eastern part of North America, in the beginning of August 1988. The numerical simulation was performed on grids with resolution of 20 and 40 km with 25 vertical levels. The emissions inventory considered in the simulation included point sources, surface biogenic sources, surface mobile sources and surface non-mobile sources. An evaluation of the model results against observations clearly indicates the ability of the system to simulate regional aspects of a tropospheric ozone episode. The model performance compares well to other models' results reported in the literature. An important achievement of this work is improving the physical realism of simulations by using highly accurate, nonoscillatory semi-Lagrangian advection transport algorithms.

1. Introduction

Tropospheric ozone is generated by photochemical reactions in the atmosphere containing NO_x species and hydrocarbons. The occurrence of high concentrations of ozone in the lower part of the troposphere is considered as one of the most important issues of air quality and tropospheric chemistry of atmospheric oxidants (Crutzen, 1988 and Davies et al., 1987). The necessary prerequisites for the formation of regional scale ozone episodes are large scale emissions of hydrocarbons and nitrogen oxide precursors and suitable meteorological conditions. Meteorological conditions promoting ozone formation are relatively well known (Guicherit and Van Dop, 1977). The experimental data indicate that the major factors are solar radiation, high air temperatures and low wind speeds. The restricted boundary layer depth is also an important factor allowing the build-up of ozone precursors.

The chemical mechanisms of tropospheric ozone

[1] Corresponding author.
* The National Center for Atmospheric Research is sponsored by the National Science Foundation.

formation are complex, but can be summarized as follows: conversion between NO and NO_2, formation of a variety of Nitrogen–containing species and accumulation of ozone. NO_2 can serve both as initiator and terminator in the chain of reactions resulting in O_3 production (Crutzen, 1988; Seinfeld, 1986).

There are several reasons for applying a computer model for an analysis of the ozone formation in the troposphere. The first one is to understand the interaction between meteorological and chemical processes in a polluted atmosphere and ultimately improve our ability to forecast ozone episodes. The second reason is a need to interpret measurements and consequently use the model as a data assimilation tool. This problem is fairly simple for passive tracers but some further study is required to generalize it for the case of complex chemical reactions (Robertson and Persson, 1992). A third reason is the potential application of the model to investigate benefits and costs of emission control strategies. The decision to reduce emissions of hydrocarbons and nitrogen compounds should be supported by the analysis performed with a comprehensive transport and chemistry model. Considering the practical importance of the problem, the numerical modelling of atmospheric oxidants was addressed by several research groups; see van Dop et al. (1987), McKeen et al. (1991) and Simpson (1993) for a discussion of existing models.

The primary objective of this paper is to present the formulation of a Chemical Tracer Model (CTM) featuring an accurate transport algorithm and comprehensive oxidants chemistry. The numerical method applied for solving the reactive transport problem is based on nonoscillatory semi-Lagrangian approximations for fluids discussed extensively in Smolarkiewicz and Pudykiewicz (1992). These algorithms preserve monotonicity (and therefore a sign) of transported variables and accurately represent the coupling between passive tracer advection and reactive chemical forcing of dependent variables.

The CTM is executed using the horizontal wind components, vertical motions, temperature, clouds and Planetary Boundary Layer (PBL) parameters calculated by the semi-Lagrangian nonhydrostatic mesoscale model discussed in detail by Tanguay et al. (1990). The meteorological model contains an extensive parameterization of physical processes including a boundary layer parameterization scheme and clouds. The coupled meteorological and tracer models were used to simulate a large scale ozone episode in the North-Eastern part of North America during the summer of 1988. The results of the numerical simulation were compared to observations in order to demonstrate the system's ability to predict the regional scale ozone episodes in the lower part of the troposphere. The model performance compares well to other models' results reported in the literature. An important achievement of the work described in this paper is improving the physical realism of simulations by using highly accurate, nonoscillatory semi-Lagrangian advection transport algorithms (Smolarkiewicz and Pudykiewicz, 1992). The errors associated with numerical diffusion were significantly reduced and the small scale structures of chemical fields are represented with better accuracy. The semi-Lagrangian algorithm employed in this study has also quite good conservation properties, the loss of mass during the simulated time of 6 days is less than a fraction of one percent.

The first section of the paper presents equations governing the reactive transport of tropospheric ozone and numerical methods used to obtain approximate solutions of these equations. The sections following the theoretical formulation describe the results of the numerical simulation, sensitivity to the changes of resolution and the model evaluation.

2. Chemical transport model

2.1. *Analytic formulation*

The chemical development of tropospheric ozone episodes involves the interaction between processes of hydrocarbon and NO_x emissions, photochemistry, 3-dimensional advection and deposition. One way to increase our understanding of this system is by applying a comprehensive model representing accurately the interaction between fluid flow and chemical reactions. The relevant reactive transport equations may be compactly written as:

$$\frac{\partial n_i}{\partial t} = -\nabla\cdot(n_i\, V) - \nabla\cdot\overline{(n_i' V')} - \nabla\cdot(n_i\, v_{di}) + Q_i - L_i n_i + S_i\,, \qquad (1)$$

where: V is fluid velocity; n_i is a number density of species i (cm^{-3}) with $i=1, \ldots, N_s$ and N_s denoting the number of chemical species; $\overline{n_i'V'}$ is the subgrid scale flux of n_i with primes and overbar denoting variables' fluctuations and ensemble average, respectively; $\nabla \equiv (\partial/\partial x, \partial/\partial y, \partial/\partial z)$; v_{di} is the diffusion velocity of species i; and S_i is the emission rate of species i. The chemical production Q_i and loss L_i terms can be written in the following form:

$$Q_i = \sum_j k^f_{i,j} n_j + \sum_{j,k} k^f_{i,jk} n_j n_k + \sum_{j,k,l} k^f_{i,jkl} n_j n_k n_l , \qquad (2)$$

$$L_i = k^r_i + \sum_j k^r_{i,j} n_j + \sum_{j,k} k^r_{i,jk} n_j n_k , \qquad (3)$$

where k^f and k^r are the forward and reverse chemical reactions rates, respectively.

For the majority of practical problems considered in meteorology, including the simulation of tropospheric oxidants, the system (1) is simplified. The molecular diffusion terms are assumed to be negligible when compared to the fluxes associated with unresolved scales . The effects of unresolved scales can be represented by empirical terms relating subgrid-scale fluxes to the gradient of grid resolved quantities $\overline{n_i'V'} = -\boldsymbol{K}\nabla n_i$, where $\boldsymbol{K}$ is the diagonal tensor of diffusion coefficients (Benoit et al., 1989). The result of these modifications is a set of equations with the empirical forcing terms describing effects of small scale processes (Pudykiewicz, 1989). The chemical kinetics coefficients depend on the thermodynamic variables such as temperature, pressure, solar radiation flux and cloud fraction (Seinfeld, 1986) and are derived from the calculations performed with the meteorological model. The emission from point sources represented by the term S_i on the right hand side of (1) is calculated as a superposition of Gaussian functions centered at actual point source locations (see eq. (14) and the accompanying discussion in Section 3 of this paper).

Idealizations of the reactive terms in (1) are far more extensive than simplifications of the transportive terms discussed above. One reason for this fact is the very large number of hydrocarbons and their complex oxidation path to ozone formation. It is not likely that all of them could be included explicitly in the simulation. The lack of reliable emission data, simplifications introduced to the dynamics of the system and computational efficiency considerations are the most important factors limiting the number of species included in our simulation. The chemical kinetics schemes used to formulate Q and L terms in equations (2) and (3) are therefore always relying on a parameterization in order to reduce the number of hydrocarbons included in the simulation . The strategies involved in the parameterization of chemistry are discussed by Seinfeld (1986).

In our simulation we employed the ADOM-II chemical mechanism which was used by Environment Canada during the assessment of an acid rain problem (MacDonald et al., 1993). The ADOM-II chemical mechanism is the result of a number of studies designed to develop and verify chemical mechanisms for atmospheric models. The original mechanism known as ADOM-I (Lurman et al., 1986) was updated to be consistent with more recent results of research in organic chemistry (Atkinson, 1990; Atkinson et al., 1992) and mechanism developed for urban airshed modelling (Carter, 1990). The updated mechanism known as ADOM-II (Acid Deposition and Oxidants Model–II) has 114 chemical reactions and 47 species. The list of chemical species included in the simulations is given in Table 1. The inorganic chemistry in the ADOM–II mechanism is very similar to that in ADOM–I mechanism. The new reactions included in ADOM–II are the explicit reactions of atomic oxygen $O(^3P)$ and $O(^1D)$, the $NO + NO + O_2$ reaction, and the $HO + HO_2$ reaction. Rate constants for the inorganic reactions are based primarily on the recommendations of DeMoore et al. (1988).

The organic chemistry is similar to that in ADOM–I, although the composition of the lumped species was updated according to more recent measurements (Jeffries et al., 1988). The emitted organic compounds in the mechanism include propane, a lumped higher alkane (ALKA), ethene, a lumped higher alkene (ALKE), toluene, a lumped higher aromatics (AROM), formaldehyde, acetaldehyde (and higher aldehydes), methyl ethyl ketone, and a lumped cresol/phenol (CRES). The emission lumping process employed is described in detail by Middleton et al. (1990). In the version of the ADOM–II mechanism used for short term regional scale studies, methane, ethane and carbon monoxide all have constant concentrations.

The daytime tropospheric chemistry is driven by the photochemical reactions induced by solar

Table 1. *List of chemical species*†

Chemical species		Contribution from surface area emissions				Point sources
Full name	Chemical symbol	Biogenic	Non-mobile	Mobile	Minor point source	Major point source
sulfur dioxide	SO_2		●	●	●	●
sulfate	SO_4		●	●	●	●
nitric oxide	NO	●	●	●	●	●
nitrogen dioxide	NO_2	●	●	●	●	●
ozone	O_3					
hydrogen peroxide	H_2O_2					
nitric acid	HNO_3					
PAN	PAN					
propane	C_3H_8		●	●	●	●
>C3 alkanes	ALKA		●	●	●	●
ethene	ETHE		●	●	●	●
>C2 alkenes	ALKE	●	●	●	●	●
toluene	TOLU		●	●	●	●
higher aromatics	AROM		●	●	●	●
formaldehyde	HCHO		●	●	●	●
acetaldehyde	ALD_2		●	●	●	●
methyl ethyl ketone	MEK		●	●	●	●
methyl glyoxal	MGLY					
general dicarbonyl	DIAL					
organic peroxide	ROOH					
O-cresol	CRES		●	●	●	●
nitrous acid	HONO			●		
alkyl nitrate	RNO_3					
isoprene	ISOP	●				
hydroperoxy radical	HO_2					
total RO_2 radicals	RO_2					
CH_3CO_3 radical	MCO_3					
ammonia	NH_3		●	●	●	●
soil dust	DUST					
oxygen-singlet D	O*SD					
atomic oxygen	O					
nitrogen trioxide	NO_3					
nitrogen pentoxide	N_2O_5					
pernitric acid	HNO_4					
hydroxyl radical	OH					
general RO_2	RO_2R					
general RO_2 #2	R_2O_2					
alkyl NO_3 RO_2	RO_2N					
phenoxy radical	BZO					
crigee biradical	CRG_1					
crigee biradical	CRG_2					
methane	CH_4					
ethane	C_2H_6					
carbon monoxide	CO					
water vapor	H_2O					
oxygen	O_2					
air	M					

† Emitted species are marked by circles.

radiation. The rate of photolytic reactions is expressed as the concentration of the photoactive species multiplied by the photodissociation rate coefficient: $J=\int I_\lambda \varepsilon_\lambda \phi_\lambda d\lambda$, where: I_λ is the actinic flux, ε_λ is the absorption cross–section and ϕ_λ is the photodissociation quantum yield. The actinic flux at a given time and altitude depends upon a number of variables, including solar zenith angle, air density, the distribution of ozone in the stratosphere, aerosol loading and cloud field. All these factors influence the absorption and scattering of light in the atmosphere. Thus, relatively complicated radiative transfer models are required to calculate actinic fluxes. The ADOM-II photodissociation rate coefficients are calculated by using tables of clear sky actinic fluxes from Peterson (1976). The calculations were performed using the radiative transfer model developed by Dave (1972). The effect of clouds on clear air photolysis rate constants was included through multiplication by a correction factor according to the method described by Chang et al. (1987).

For simplicity of further discussion, it is convenient to write (1) in the symbolic form:

$$\frac{D\Psi}{Dt}=F_c(\Phi, \Psi, t). \tag{4}$$

Here Φ is a vector of fluid variables including wind, temperature, humidity and cloud water (the fluid velocity V is identical to some three components of Φ); $\Psi\equiv(\Psi_1, \ldots, \Psi_{N_s})$ is a vector of chemical variables (mixing ratios of chemical species); and $D/Dt\equiv\partial/\partial t+V\cdot\nabla$. The vector F_c combines all chemical kinetics, the emission of the chemical species and diffusion terms:

$$F_c(\Phi, \Psi, t)=\nabla K\nabla\Psi + F_c^k(\Phi, \Psi, t)+S/\rho, \tag{5}$$

where $S\equiv(S_1, \ldots, S_{N_s})$, and ρ is air density. The term describing the chemical kinetics given by equations (2) and (3) is denoted as F_c^k. Each component of this vector depends on chemical and dynamic variables, that is,

$$F_c^k=(F_c^1(\Phi, \Psi, t), \ldots, F_c^{N_s}(\Phi, \Psi, t)).$$

The reactive transport model (4) is coupled with a meteorological model that can be compactly written:

$$\frac{D\Phi}{Dt}=F_f(\Phi, t). \tag{6}$$

which symbolizes a set of prognostic equations for momentum, temperature, moisture and cloud water. Here, the vector F_f does not depend on chemical variables and hence, the equation systems (4) and (6) could be solved separately. This approximation is quite well justified in the case of tropospheric chemistry over a time scale of a few days because the chemistry is not affecting the dynamic variables in an evident way. The situation is thus opposite to the stratospheric problems where perturbations of the radiative transfer due to chemical constituents affect the temperature field and consequently the flow field.

2.2. *Finite difference approximations*

The semi-Lagrangian algorithm adopted for integrating the system of reactive transport equations (4) can be written according to the theory described by Smolarkiewicz and Pudykiewicz (1992) in the following compact form:

$$\Psi(x_i, t_1)=\Psi_0+\int_T F_c(\Phi, \Psi, t)dt. \tag{7}$$

The subscript $_0$ in the first term on the right hand side refers to a field value at the departure point (x_0, t_0) of the trajectory arriving at the grid point (x_i, t_1); here, it denotes an elaborate, at least second-order-accurate, nonoscillatory interpolation algorithm that is built upon forward-in-time Eulerian advection schemes for integrating the homogeneous transport equation with constant coefficients (Smolarkiewicz and Grell, 1992; Smolarkiewicz and Pudykiewicz, 1992). The nonoscillatory (monotonicity and/or sign preservation) property is important for the computational stability and overall accuracy of approximations to reactive transport problems with nonlinear chemistry (cf. section 15.5.1 in Brasseur and Madronich, 1992). In this paper, the departure points $x_0(x_i, t_1)$ are evaluated from the trajectory equation $Dx/Dt=V$ using a second-order-accurate, implicit algorithm based on a Taylor series expansion (Smolarkiewicz and Pudykiewicz, 1992, section 4b and appendix). [Optionally, the CTM admits the fourth-order Runge-Kutta scheme for trajectory evaluation.] The second term on the right hand side of (7) symbolizes the integral along a flow trajectory of all forcings which enter the governing problem (4). The CTM admits several particular approximations of this

integral. Below, we discuss the approximation employed in this paper, whereas other available options will be reported elsewhere.

The set of eqs. (4) governs processes with very different time scales. The time scale of advection and slow chemical reactions is many orders of magnitude larger than the time scale of the fastest reactions. It is convenient to rewrite the forcing term of (4) in the form separating processes characterized by different time scales:

$$\boldsymbol{F}_c(\boldsymbol{\Phi}, \boldsymbol{\Psi}, t)=\boldsymbol{F}_c^d(\boldsymbol{\Phi}, \boldsymbol{\Psi}, t)+\boldsymbol{F}_c^q(\boldsymbol{\Phi}, \boldsymbol{\Psi}, t) + \boldsymbol{F}_c^k(\boldsymbol{\Phi}, \boldsymbol{\Psi}, t). \quad (8)$$

Here $\boldsymbol{F}_c^d \equiv \nabla_H \boldsymbol{K}_H \nabla_H \boldsymbol{\Psi}$ is the vector of forcings associated with horizontal diffusion (subscript $_H$ refers to horizontal derivatives and appropriate elements of the tensor $\boldsymbol{K}$); $\boldsymbol{F}_c^q \equiv (\partial/\partial z(K_{zz}\partial/\partial z)\boldsymbol{\Psi})+\boldsymbol{S}/\rho$ is the forcing due to the combined effect of emissions from point sources and vertical diffusion. The term describing the chemical kinetics is denoted as $\boldsymbol{F}_c^k$.

The governing problem (4) is solved in (7) subject to boundary conditions representing the flux balance between deposition of chemical species and surface emissions:

$$K_{zz}\frac{\partial \boldsymbol{\Psi}}{\partial z}-\boldsymbol{v}_{dep}\boldsymbol{\Psi}+\boldsymbol{f}_{em}/\rho=0, \quad (9)$$

where $v_{dep}=(v_{dep}^1, \ldots, v_{dep}^{N_s})$ is the deposition velocities vector, and $\boldsymbol{f}_{em}=(f_{em}^1, \ldots, f_{em}^{N_s})$ denotes vector of surface emissions.

The deposition velocity v_{dep}^i is calculated following the formulation of Wesely and Hicks (1977) and McKeen et al. (1991). The inverse of deposition velocity is the sum of the aerodynamic resistance r_a and the surface resistance r_s^i: $1/v_{dep}^i=r_a+r_s^i$. The surface resistances in our calculations are constant in time and the values of r_s^i for deposited species are the same as in McKeen et al. (1991).

The separation of the time scales justifies rewriting (7) in the spirit of process splitting—a common approach in modelling complex, interacting processes in fluids (section 4.6 in Oran and Boris, 1987). The formal semi-Lagrangian integral (7) of the set of reactive transport equations (4) along a flow trajectory is approximated with the sequence of two computationally simpler tasks:

$$\tilde{\boldsymbol{\Psi}}(\boldsymbol{x}_i)=\boldsymbol{\Psi}_0+\int_T [\boldsymbol{F}_c^d(\boldsymbol{\Phi}, \boldsymbol{\Psi}, t)+\boldsymbol{F}_c^q(\boldsymbol{\Phi}, \boldsymbol{\Psi}, t)]\,dt, \quad (10)$$

$$\boldsymbol{\Psi}(\boldsymbol{x}_i, t_1)=\tilde{\boldsymbol{\Psi}}(\boldsymbol{x}_i)+\int_{t_0}^{t_1} \boldsymbol{F}_c^k(\boldsymbol{\Phi}, \tilde{\boldsymbol{\Psi}}, \tau)\,d\tau. \quad (11)$$

Here, (10) represents the combined effect of advection and forcings due to mixing and emission integrated along the flow trajectory, and (11) accounts for chemical reactions at each grid point of the discrete mesh. The trajectory integral in (10) is approximated using an implicit trapezoidal rule for vertical diffusion and emission terms and explicit forward formulae for the horizontal diffusion. This leads to the numerical approximation:

$$\tilde{\boldsymbol{\Psi}}(\boldsymbol{x}_i)=\boldsymbol{\Psi}_0+\Delta t\boldsymbol{F}_c^d(\boldsymbol{x}_0, t_0)+\tfrac{1}{2}\Delta t(\boldsymbol{F}_c^q(\boldsymbol{x}_0, t_0) + \boldsymbol{F}_c^q(\boldsymbol{x}_i, t_1)), \quad (12)$$

where $\Delta t \equiv (t_1-t_0)$. Taking into account the definition of $\boldsymbol{F}_c^q$ in (8), (12) represents the set of $N_s*N_x*N_y$ one-dimensional Helmholtz equations subject to the boundary conditions in (9). It can be readily inverted using elementary methods of linear algebra.

In contrast to (10), the grid-point integral over Δt in (11), in general, has no simple compact form as that in (12). Formally, (11) may be interpreted as a solution to:

$$\frac{\partial \boldsymbol{\Psi}}{\partial t}=\boldsymbol{F}_c^k(\boldsymbol{\Phi}, \boldsymbol{\Psi}, t), \quad (13)$$

evaluated independently at each grid point after accounting for tendencies associated with transportive forcings in (12). The selection of the algorithm used for the solution of (13) is now mostly a matter of requirements associated with the specific chemistry scheme. One possibility is the use of the Gear type scheme (Hindmarsh, 1983). The second choice is an application of the more efficient but less accurate asymptotic algorithm described by Young and Boris (1977) which was employed in calculations discussed in the remainder of this paper. The chemistry calculation using (13), in general, requires a much smaller time step than Δt in (12). This discrepancy of time steps is resolved by nesting the chemistry integration within the time interval used for dynamical calculations. This nesting permits a flexible adjustment of the time step of the chemistry integration according to the changes in the stiffness of the system.

The numerical approximations employed for the solution of dynamic equations (6) are discussed extensively by Tanguay et al. (1990) in the context of the formulation of the meteorological model. The set of dynamic equations is solved on a polar stereographic projection in the terrain following coordinate system, commonly used in mesoscale meteorological models (Gal-Chen and Sommerville, 1975). The main features of the numerical approximations are standard; e.g., they include the three-time-level, semi-Lagrangian semi-implicit integration scheme of Robert et al. (1985). The model employs the usual parameterization of the PBL based on similarity theory (Businger et al., 1971). The set of dynamic equations is complemented by additional equations predicting the length and velocity scale of unresolved motions (Benoit et al., 1989). The results of this subgrid-scale model are used to calculate the turbulent diffusion coefficients. The cloud field is represented by standard parameterizations described by Sundqvist (1988). The verification of this scheme shows that it is sufficiently accurate for regional scale modelling (Pudykiewicz et al., 1992).

The meteorological model is executed in nested mode with the time dependent boundary conditions provided by the objective analysis or another meteorological model with a coarser grid. The nesting scheme used is based on the traditional method described by Davies (1976) and investigated further in the context of meteorological forecast models by Yakimiw and Robert (1990).

3. Simulation of a regional scale ozone episode

The numerical model summarized in the preceding section, has been employed to simulate the evolution of tropospheric ozone for the case of the major smog episode over the north-eastern part of North-America. The simulated event occurred during the six day period between August 1 and 6 of 1988. The meteorological situation was characterized by a stable high pressure system with relatively weak winds, negligible cloud cover and high temperatures at the surface. The ozone concentrations reached a relatively high level and a well defined regional scale ozone episode was observed. The additional rationale for simulating this event was the fact that the summer of 1988 was the time selected for the Eulerian Model Evaluation Field Study (EMEFS) (MacDonald et al., 1993) so the measurements of concentrations of ozone and ozone precursors for this time are readily available (McNaughton et al., 1994).

The meteorological model was run first for the time interval of 8 days starting on July 30. The simulation was initiated two days before the beginning of the ozone episode in order to spin-up variables characterizing the chemical part of the system. The horizontal grid with a resolution of 40 km used in the meteorological simulation was defined on a Polar Stereographic projection Fig. 1, and 25 vertical levels were employed for the numerical solution of the model equations. Placement of the levels was such that levels within the atmospheric boundary layer were separated by small distances and the separation of the levels was greater in the free atmosphere.

The grid of the meteorological model was nested within the global scale grid and the time dependent boundary conditions were obtained from the objective analysis system of the Canadian Meteorological Centre (Mitchell et al., 1996). The surface wind and surface pressure at the beginning and at the end of the simulated ozone episode are shown in the Fig. 2. The meteorological simulation reflected realistically relatively calm winds over the source regions, a high temperature at the surface and large insolation during daylight hours.

After completing the meteorological model run, the 3-D simulation of the regional scale NO_x/VOC chemistry was performed on a grid with a uniform resolution of 40 km, imbeded within the grid of meteorological model. The corresponding horizontal grid was 61*61 points. The vertical resolution of the tracer model was the same as the resolution employed during the execution of the meteorological driver.

The emission data base used in our simulation was assembled from the 1985 NAPAP Emission Inventory (Version 2), (U.S. EPA , 1989). The emission information includes contributions from major point sources as well as gridded area emissions given at hourly intervals. The spatial resolution of the area emission was around 20 km on a Polar Stereographic projection. The gridded area emissions consist of biogenic, mobile, non–mobile sources, and minor point sources grouped

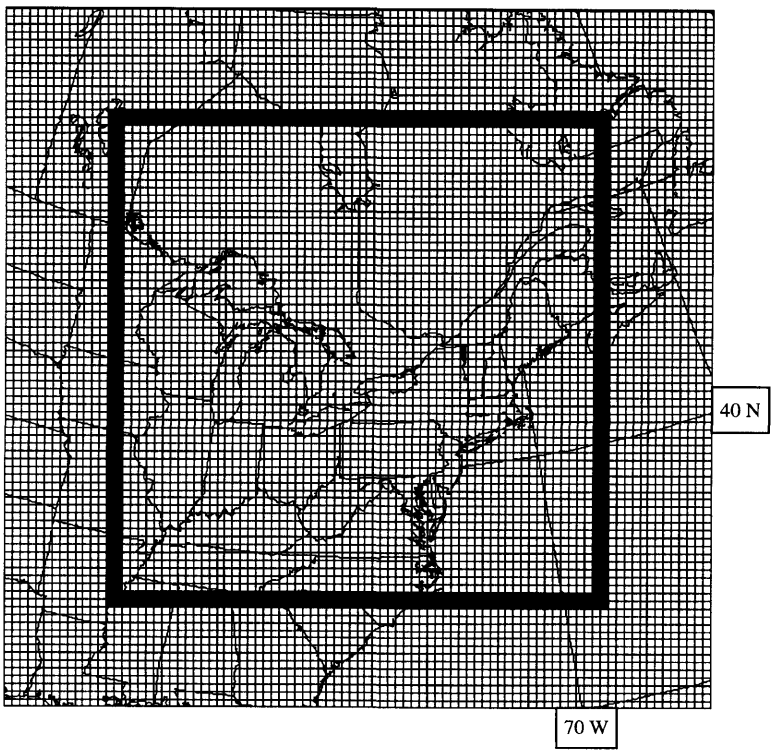

Fig. 1. The horizontal mesh of the meteorological model. The thick frame indicates the computational domain of the tracer model.

as area sources. All emission information is time dependent. Date specific, hourly emission rates were used for biogenic emissions, whereas seasonal hourly rates, broken into a weekday, Saturday, Sunday classification were used in the case of anthropogenic area emissions. The emission rates from major point sources were calculated for each hour using the multiplicative factors specified separately for a weekday, Saturday and Sunday. The time variability of the emission from major point sources included also multiplicative factors accounting for seasonal emission changes. The total summer day emission of NO_x and VOC within the model domain is 1.86×10^7 and 5.26×10^7 kg respectively.

Point source emissions were represented in the model as a sum over Gaussian distributions centered at actual source locations:

$$\boldsymbol{S}(\boldsymbol{x}, t)=\sum_k \boldsymbol{E}_k(t) A_k \prod_{m=1}^{3} \exp\left(\frac{-(x_m-x_{m,k})^2}{2\sigma_{m,k}^2}\right). \quad (14)$$

Here $\boldsymbol{E}_k$ denotes the vector of species emitted from the kth source, $\boldsymbol{A}_k$ is the normalization constant for the kth source, $x_{m,k}$ denotes mth component of the position vector of the kth source, and $\sigma_{m,k}$ is a set of parameters describing the subgrid-scale dispersion of the material released from the stack. The parameters of the source function (14) are dependent on the stability calculated by the meteorological model using the Pasquill-Gifford relations (Gifford, 1961; 1968). The area average emission and deposition of species were represented by the lower boundary conditions of the tracer equations using the method discussed by Pudykiewicz (1989).

The regional atmospheric tracer model was executed for the same time interval as the meteorological model. All calculations were performed using the second-order-accurate nonoscillatory remapping algorithm (Smolarkiewicz and Grell, 1992) in (12). The time step in (12) was 1 h (resulting in Courant numbers well exceeding unity during advection dominated meteorological

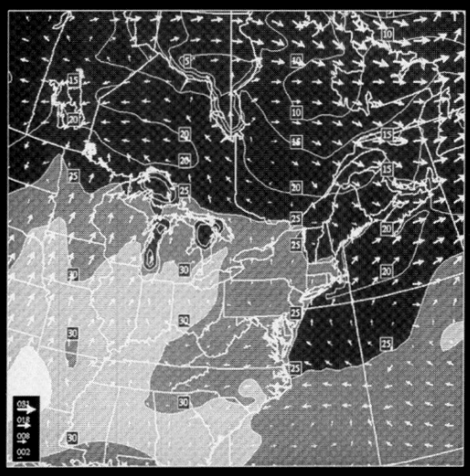

a

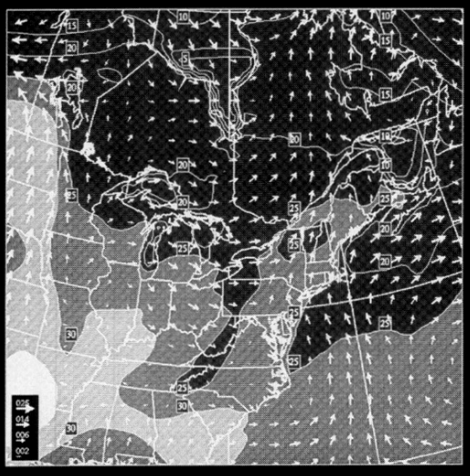

b

Fig. 2. The wind and temperature fields simulated by the meteorological model at anemometer level at 18 GMT: (a) 2 August, (b) 6 August 1988.

situations) whereas the chemistry system (13) employed a dynamically adjustable time step varying according to the stiffness of the chemistry system.

The simulated ozone fields at the anemometer level, defined at 10 m above the surface are depicted in Fig 3. The fields are shown four hours after noon time, Eastern Local Time (20 GMT), for each day between 1 and 6 August. The elevated ozone concentrations, exceeding 60 ppb, are simulated over a large part of North Eastern North America. The maximum ozone concentrations occurred on 2 and 3 August (Fig. 3b, c) reaching values of over 200 ppb. The formation of ozone during the first stage of the smog episode was dominated mostly by local scale meteorological processes, dry deposition and chemistry. During the following 2 days, ozone concentrations started to decline (Fig. 3d, e). The ozone plumes changed shape in response to an increase of the wind speed. Subsequently, the large ozone concentrations were drastically reduced on August 6 (Fig. 3f), this day could be considered as the end of the ozone episode. The time variability of the computed ozone concentrations is consistent with measurements (Fig. 5) and it shows that the model simulates correctly the coupling of the complex chemistry with the meteorological forcings.

The amount of ozone that is photochemically produced within the specific model subdomain in relation to transport was strongly dependent on the distribution of emission sources. In the areas of intensive emission of ozone precursors the predominant source of ozone was the local photochemical generation. In the areas located even at large distances downwind from the major emission centers, the model shows that a significant amount of ozone was transported from the regions with large emissions.

The characteristic feature of the ozone distribution obtained from the model simulation is the presence of well formed plumes centered around major emission areas. The shapes of these plumes were varying with changes of the predominant flow. The most prominent are two large scale ozone plumes depicted in Fig. 3c. The first one is oriented along the axis of Windsor-Quebec corridor in Canada and the second one along the East Coast of the United States. The presence of these plumes is associated with very low wind speeds, intensive vertical mixing within the Planetary Boundary Layer and high temperatures.

The analysis of Fig. 3c shows that the ozone plume topology on the regional scale under calm conditions is dominated by the emission field, dry deposition processes and vertical mixing within the convective boundary layer. The maximum ozone concentrations coincide with areas of large emission of ozone precursors and enhanced vertical mixing. The opposite situation could be observed on 4 and 5 August (Fig. 3d, e) when the wind speed increased and the ozone plume became dominated by the horizontal advection. The

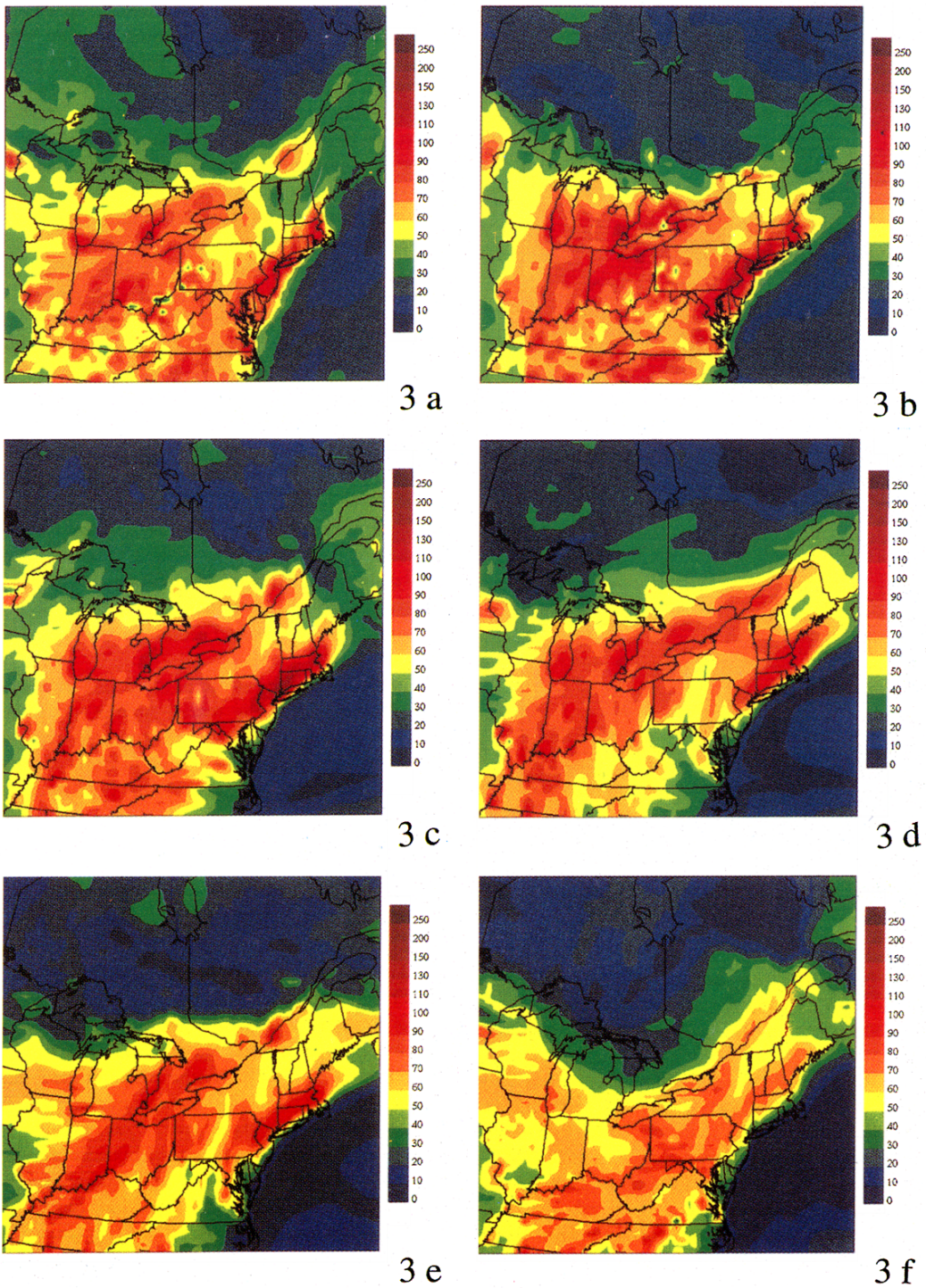

Fig. 3. The ozone field at the anemometer level simulated by the tracer model run with 40 km resolution. All fields are valid at 20 GMT: (a) 1 August, (b) 2 August, (c) 3 August, (d) 4 August, (e) 5 August, (f) 6 August 1988.

increase of the wind speed was associated with lower ozone concentrations in the area of sources.

The general conclusion from the qualitative evaluation of the model results depicted in Fig. 3 is that the ozone field on a regional scale is formed under two different meteorological regimes; the first one dominated by local processes such as emissions, boundary layer mixing and dry deposition and the second one governed mostly by the advection. The second regime is usually associated with much smaller ozone concentrations over the model domain.

4. Model evaluation

The evaluation of the model was performed for the surface ozone field. The time interval considered was 6 days starting from 1 August 00 GMT. The experimental data for model evaluation was provided by a set of 70 stations located within the area surrounded by the thick frame in Fig. 1. The stations selected for our study were part of 5 networks which were operated under independent sponsorship during EMEFS (McNaughton et al., 1994).

The measured surface ozone concentrations were compared to the output of the tracer model saved every 1 h during the 6-day simulation. This particular time sampling frequency was selected because the averaging period for ozone measurements was equal to 1 h for all the considered stations. The model values at the points corresponding to experimental sites were obtained from the nearest grid points of the computational mesh from the model level corresponding to the anemometer height. The comparison of simulated and observed ozone concentrations for the set of stations depicted in Fig 4 is shown in Fig. 5.

One of the most critical aspects of the ozone formation in the lower troposphere is its dependence on the diurnal cycle. The presence of the diurnal cycle is reflected realistically in the time series depicted in Fig. 5. The model simulates also quite well the general trend of the observed concentrations in response to the changing meteorological conditions. The model evaluation shown in the Figs. 5d, and 5g, h is very good for all days of the smog episode. The scores for other stations vary significantly with time. The biggest error is

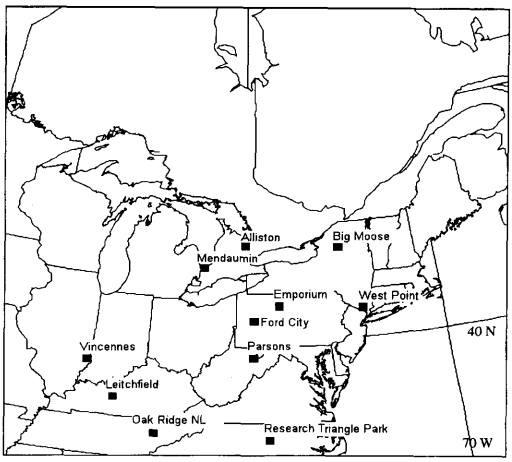

Fig. 4. The map showing locations of stations for which model evaluation is presented in graphical form.

observed during the first two days of the smog episode (Figs. 5c, i).

The summary of the statistical data evaluation for the group of selected stations indicated in Fig. 4 is given in the Table 2. The second column in the table shows the correlation coefficient. With the exception of one station, the correlation coefficient is between 0.65 and 0.90. This fact indicates that the model results represent observations with acceptable accuracy. The average ozone concentrations calculated for observation and the model are shown in column 3 and 4 respectively. The analysis of average values indicates that the model bias defined as:

$$B = \sum_i (\Psi_{\text{simulated}}(t_i) - \Psi_{\text{observed}}(t_i))/N$$

$$= (\bar{\Psi}_{\text{simulated}} - \bar{\Psi}_{\text{observed}})$$

averaged over the ensemble of stations considered is less than 6 ppb. This result is very good, considering the complexity of the simulated system.

The standard deviation of observed and simulated ozone concentrations is shown in columns 5 and 6 respectively. The variability of experimental data is also comparable to the model values. This fact reflects that the model simulates relatively well all the range of ozone concentrations — from very low, observed at night up to the peak values occurring during afternoon. This fact indicates a significant improvement of the realism of simula-

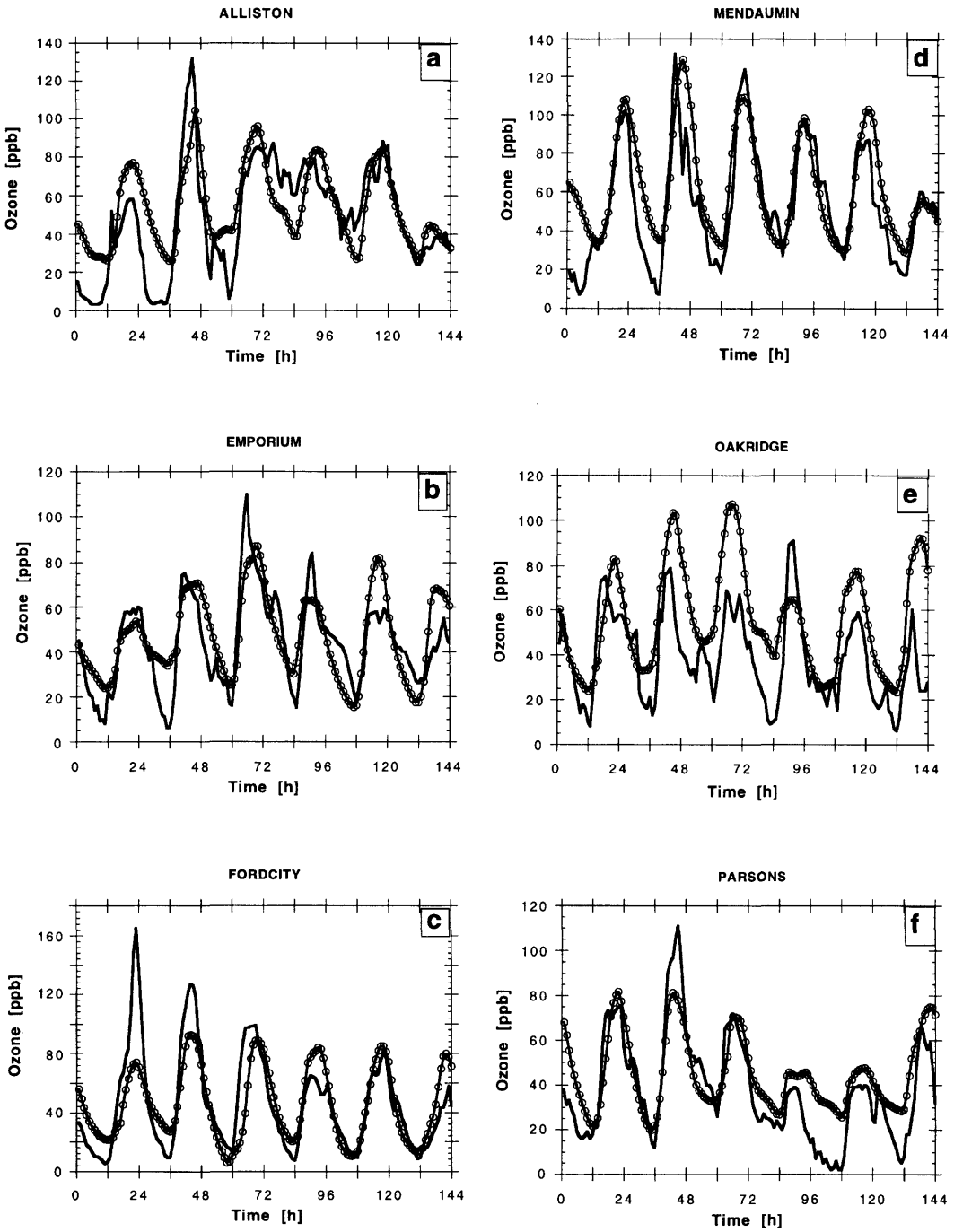

Fig. 5. The comparison of the observed and simulated ozone concentrations shown in [ppb] units. The observed values are indicated by a solid line and the model results are depicted by line with circles. The units of the horizontal axis are hours starting from 00 GMT on 1 August 1988.

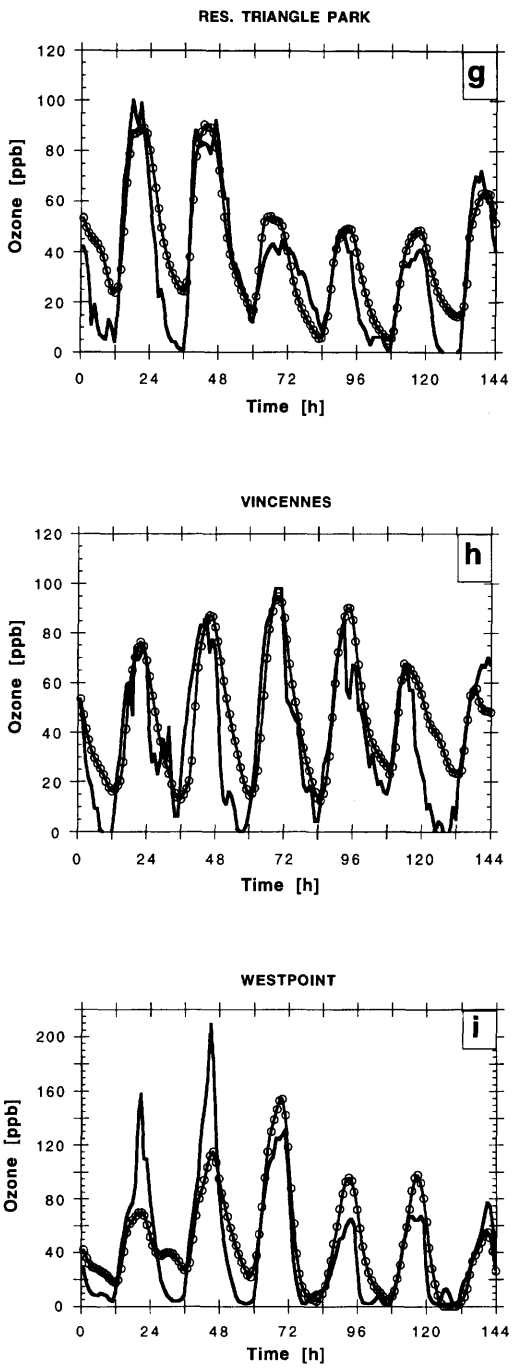

Fig. 5. (cont'd).

tion when compared to other models using ADOM-II chemistry scheme (MacDonald et al., 1993).

The model performance demonstrated by the data in the Table 2 and time series depicted in Fig. 5 is in general quite good. The small discrepancies between the model and observation could be attributed to inadequate representation of local scale meteorological processes due to the errors of objective analysis providing the lateral boundary conditions for the meteorological model and errors of physical parameterizations included in the model. The most evident examples are provided by the parameterization of vertical fluxes employed in meteorological and CTM models. Our analysis indicates that the parameterization of the structure of the boundary layer calculated by the meteorological model affects the vertical mixing of tracers and deposition processes and it is therefore very important for a realistic ozone simulation.

The other important process affecting accuracy of the simulation is the transport of tracers in Cumulus clouds (Feichter and Crutzen, 1990). Though not as obvious in the PBL as in the upper troposphere, it can influence, however, the ozone concentrations observed at the surface.

In addition to physical processes, the disagreement between the predicted and simulated ozone values could be also attributed to the lack of complete information about the time dependence of emission rates, especially from the biogenic sources.

The major model deficiency is the relatively poor prediction of the peak ozone concentrations for some stations for 1 and 2 August. There are several explanations of this fact. In the past it was suggested that the problem with prediction of high ozone concentrations is associated with chemistry scheme employed. After the closer examination of the results it becomes evident that the discrepancy seen in Fig. 5 can not be attributed to the chemistry scheme alone. The most likely explanation is that the model performance is affected by several factors such as chemistry scheme, physical parameterizations included in the model, emission data and finally the specific procedure used for the model evaluation.

The last factor is particularly important and it requires some additional explanation. The fact that measurements are done at a point and model

Table 2. *General statistical data describing simulated and observed ozone concentrations*‡

Station	ρ	$\bar{\Psi}_{observed}$	$\bar{\Psi}_{simulated}$	$\sigma_{observed}$	$\sigma_{simulated}$
Alliston	0.7650	48.56	54.01	28.31	20.38
Big Moose	0.7329	47.44	45.86	17.14	17.09
Emporium	0.7646	43.85	46.76	20.42	18.44
Ford City	0.7837	45.99	45.38	33.63	25.04
Leitchfield	0.5768	46.09	54.05	17.49	17.58
Mendaumin	0.8024	52.73	62.21	28.29	26.58
Oak Ridge	0.6613	39.06	55.98	19.64	22.88
Parsons	0.8316	37.92	44.89	23.26	16.54
Triangle Park	0.8851	34.25	40.33	26.93	22.69
Vinncenes	0.7960	38.96	45.90	27.04	22.72
West Point	0.8283	41.72	47.88	44.27	35.84

‡ ρ indicates the correlation coefficient, $\bar{\Psi}_{observed}$ the observed ozone concentration (ppb), $\bar{\Psi}_{simulated}$ the simulated ozone concentration, and $\sigma_{observed}$ and $\sigma_{simulated}$ the standard deviation of the observed and simulated values of ozone concentration respectively.

results are averages over grid boxes might have an influence on the time series shown in Fig. 5. In addition to the problems with spatial sampling we could expect that the different averaging periods between the CTM and measurements could have some impact on model evaluation. The time sampling error is probably not the major problem of the discrepancy in ozone peak value shown in Fig. 5 because both model and measurements had the same time averaging period of 1 h.

In order to verify the importance of the issue of the spatial sampling error we will consider the comparison of the model results to observations for West Point (Fig. 5i). The model underpredicts the ozone peak concentration on August 2nd by about 100 pbb. Examination of the horizontal map shown in Fig. 3b shows that the model produces values consistent with the observation at West Point at the distance equivalent to 1 mesh interval, Fig. 6. The model error for 2 August at the measurement site located in West Point is associated therefore with a sampling error, not with the intrinsic properties of the chemistry scheme.

This fact is particularly important because in the past it was suggested that the ADOM-II chemistry mechanism underpredicts the maximum and overpredicts the minimum ozone concentration values (MacDonald et al., 1993). The comparison between model prediction and observation depicted in Fig. 6 clearly demonstrates that the chemistry scheme responds correctly to meteorological forcings and the model described in this

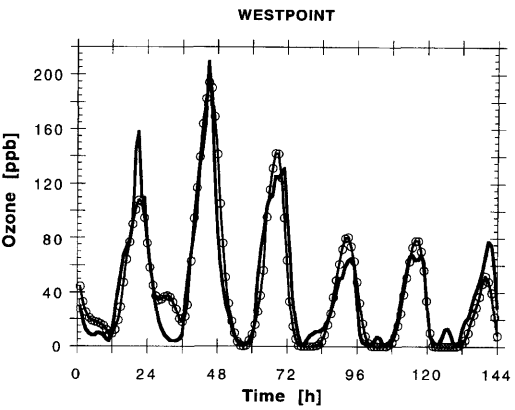

Fig. 6. Same as Fig. 5i but the simulated ozone concentrations at the Westpoint site were obtained not from the nearest grid point but from the grid point located at the distance of one mesh interval South.

study is able to reproduce the full range of observed ozone concentrations.

The sampling error observed at Westpoint suggests the need to examine the model sensitivity to the changes of resolution. In order to investigate how the accuracy of the simulation depends on the grid spacing, the meteorological and chemical transport models were rerun on the grid with resolution of 20 km. The general conclusion from the comparison of results of both runs is that doubling the model resolution is not leading to a drastic change in the simulated ozone field. This

conclusion is somewhat contrary to what was expected in the past.

After a closer analysis of the scales of processes involved in the ozone formation it is possible to explain this fact. The major meteorological factors controlling ozone formation are related to synoptic scale forcings which are represented with the same accuracy either on 40 or 20 km grids. Both resolutions, however, are not sufficient to represent realistically finer scale effects like thermal circulation associated with horizontal temperature gradients, local perturbations of the Planetary Boundary Layer and small scale features of the emission fields. In order to simulate realistically these fine scale effects the resolution of the model should be reduced probably to less than 5 km.

The major limitation preventing a numerical simulation of the regional scale ozone episode with this resolution is the availability of emission data and a parameterization of subgrid-scale processes in the meteorological model. The run of the meteorological model with this resolution is also quite difficult to justify considering the present resolution of the objective analysis system.

After examining the model response to changes of grid spacing, it is important to examine the model sensitivity with respect to the emission data. Some emission data are not known with sufficient certainty. A particularly difficult problem is associated with the evaluation of the biogenic emissions. In order to investigate the influence of the uncertainty of the emission data on the model results, we performed a series of sensitivity experiments changing the emission data for isoprene. The perturbation to the emission consisted in increasing the maximum fluxes of isoprene by 50%. This value represents the lower bound of the uncertainty of the estimate of isoprene emission.

Results of the simulation performed using the modified emission field shows that the peak ozone concentrations are represented with good accuracy. The sunrise values of ozone are simulated, however, with smaller accuracy compared to the non–perturbed run. The simple enhancement of the emission of isoprene is thus not sufficient to increase the realism of ozone prediction. Considering, however, the model sensitivity to the emission of isoprene, more effort should be directed towards improving emission information.

It is also important to note that the model applications for the evaluation of the emission control strategies should be based on the ensemble of simulations utilizing various perturbations of the emission data. This ensemble forecast of the chemical fields is essential to estimate the model uncertainty associated with the emission and meteorological forcings.

The comparison of the accuracy of the oxidants model to other models simulating atmospheric tracers could be quite instructive in order to explain sources of the model error. The accuracy of the model reported in this paper compares well with the typical accuracy of the atmospheric models simulating single tracer transport. The average value of the correlation coefficient for the simulation of the ozone field reported in this paper is 0.77 whereas the best models simulating fairly simple nonreactive tracer transport during the ATMES experiment (Klug et al., 1992) had an average correlation coefficient between 0.68 and 0.78.

When compared to other models simulating atmospheric oxidants, the CTM described in this paper performs better by being able to simulate realistically the full range of ozone concentrations from very small up to peak values. Also the average correlation coefficient is slightly higher than the typical values reported for other models such as the model described by McKeen et al. (1991). It is true to say that the nonlinear atmospheric oxidants model can not be considered to be realistic just because the values of the correlation coefficient are high. However, the high values of correlation coefficients combined with the realistic simulation of temporal trends and extreme ozone concentrations are significant manifestations of the realism of the simulation.

The good model performance in simulating reactive tracers should be considered a success because of a significant increase of complexity of forcing terms in the transport equations. This fact points to the noticeable increase of the accuracy of the tracer models which is possible due to the improved numerical techniques.

The model evaluation presented in this section is an indication of the feasibility of the semi-Lagrangian method for simulating reactive atmospheric flows on a regional scale. It is important to note, however, that the simulation of a single ozone episode is not sufficient to draw final conclusions concerning the model applicability for evaluating emission control strategies. It is relatively

well known that the performance of atmospheric oxidants models can vary quite drastically with different meteorological conditions (Simpson, 1993). Although the current results are encouraging, more meteorological cases are needed in order to evaluate the model with higher certainty and estimate errors associated with meteorological data used for calculation. Statistical data evaluation will be important to separate the sources of error associated with meteorological and emission data. These facts are important to consider when the atmospheric oxidants model is used for an emission control scenario evaluation. In our opinion, this application requires an extensive selection of meteorological scenarios in order to produce meaningful results. This evaluation will be performed in the future.

5. Conclusions

In order to investigate the formation and evolution of tropospheric ozone, a semi-Lagrangian transport model with complex chemistry was developed. The model was interfaced with a mesoscale meteorological model and a set of meteorological data assimilation programs. The calculations were performed using an extensive data base of anthropogenic and biogenic emissions of nitrogen species and volatile organic compounds.

Our experiments show that the numerical simulation of the regional scale ozone episode performed with this system of models is able to reproduce the main features of the observed ozone field. The general pattern of the ozone field observed at the surface is simulated realistically. The response of the ozone field to changing meteorological conditions is also consistent with the experimental data. The model evaluation for the set of selected stations indicates that evaluation scores are high. These scores are in fact equivalent to, or better than the scores of models simulating atmospheric transport of non-reactive tracers. This fact is encouraging considering the complexity of meteorological and chemical processes involved in the formation of the tropospheric ozone.

The issue of parameterization of unresolved scales is important in the simulation of atmospheric chemistry. Both the mixing of atmospheric tracers in the vertical direction and the deposition taking place at the surface are strongly dependent on small scale processes. The most important factor limiting the accuracy of the simulation of atmospheric oxidants is the accuracy of the parameterization of subgrid scale processes. This fact is reflected by the variability of the model results which is slightly smaller than the variability of the experimental data. The relatively simplistic parameterization of the vertical turbulent mixing and dynamics of the PBL is the most possible explanation of this fact. The main concern for future research should be, therefore, to improve the parameterization of small scale processes in the model. An improved parameterization of physical processes will require higher grid resolution and a more accurate data assimilation system.

In addition to the work with more realistic parameterizations of small scale processes, some additional effort is still required to increase the accuracy of the emission information. Particularly important is the need to create a better parameterization of biogenic emissions which is still not known with sufficient accuracy. In light of experiments indicating large model sensitivity to biogenic emissions of the isoprene, the solution of this problem is particularly important for the model application for evaluating the effectiveness of emission control. The advances in the parameterization of the subgrid scale processes and more accurate emission databases could be easily introduced in the framework of the modelling system described in our paper.

The performance of the model described in this paper compares well to other models simulating atmospheric oxidants. This fact could be attributed mostly to the nonoscillatory numerical scheme which guaranties preservation of monotonicity (and therefore a sign) of transported variables and allows an accurate representation of the coupling between passive tracer advection and reactive chemical forcing of dependent variables.

The important conclusion from the study is, therefore, that elimination of numerical errors is critical for an accurate simulation of ozone chemistry and realistic representation of small scale structures of chemical fields. Considering additionally that the numerical algorithms employed are very efficient, further development of physical parameterizations of the model will significantly improve our understanding of the tropospheric ozone problem.

REFERENCES

Atkinson, R. 1990. Gas-phase tropospheric chemistry of organic compounds: a review. *Atmos. Environ.* **24A**, 1–41.

Atkinson, R., Baulch, D. L., Cox, R. A., Hampson, R. F., Kerr, J. A. and Troe, J. 1992. Evaluated kinetic and photochemical data for atmospheric chemistry: supplement IV. *Atmos. Environ.* **26A**, 1187–1230.

Benoit, R., Cote, J. and Mailhot, J. 1989. Inclusion of TKE boundary layer parameterization in the Canadian regional finite-element model. *Mon. Wea. Rev.* **117**, 1726–1750.

Brasseur, G. P. and Madronich, S. 1992. Chemistry-transport models In: *Climate system modeling*, ed. K. E. Trenberth. Cambridge University Press.

Businger, J. A., Wyngaard, J. C., Izumi, Y. and Bradley, E. F. 1971. Flux-profile relationships in the atmospheric surface layer. *J. Atmos. Sci.* **28**, 181–189.

Carter, W. P. L. 1990. A detailed mechanism for the gas-phase atmospheric reactions of organic compounds *Atmos. Environ.* **24**, 481–518.

Chang, J. S., Brost, R. A., Isaksen, I. S. A., Madronich, S., Middleton, P., Stockwell, W. R. and Walcek, C. J. 1987. A 3-dimensional eulerian acid deposition model: physical concepts and formulation. *J. Geophys. Res.* **92**, 14681–14700.

Crutzen, P. J. 1988. Tropospheric ozone: an overview. In: *Tropospheric ozone,* ed: I.S.A. Isaksen, D. Reidel Publishing Co.

Dave, J. V. 1972. *Development of programs for computing characteristics of ultraviolet radiation.* Final report under contract NAS 5–21680, NASA Report CR–139134. National Aeronautics and Space Administration, Goddard Space Flight Center, Greenbelt, Maryland, NTIS # N75–10746/6SL.

Davies, H. C. 1976. A lateral boundary formulation for multi-level prediction models. *Quart. J. R. Met. Soc.* **102**, 405–418.

Davies, T. D., Kelly, P. M., Brimblecombe, P. and Gair, A. J. 1987. Surface ozone concentrations and climate: preliminary analysis. In: *Proceedings of the WMO Conference on Air pollution modelling and its application*, vol 2, Rep. WMO/TD 187, 348–356.

DeMoore, W. B., Sander, S. P., Molina, M. J., Golden, D. M., Hampson, R. F., Kurylo, M. J., Howard, C. J. and Ravishankara, A. R. 1988. *Chemical kinetics and photochemical data for use in stratospheric modelling, evaluation number 8.* National Aeronautics and Space Administration, Jet Propulsion Laboratory California Institute of Technology, Pasadena, California.

Feichter, J. and Crutzen, P. J. 1990. Parameterization of of vertical tracer transport due to deep cumulus convection in a global transport model and its evaluation with Ra^{222} measurements. *Tellus* **42B**, 100–117.

Gal-Chen, T. and Sommerville, R. C. 1975. On the use of a coordinate transformation for the solution of Navier-Stokes equations. *J. Comp. Phys.* **17**, 209–228.

Gifford, F. A. 1961. Use of routine meteorological observations for estimating atmospheric dispersion. *Nucl. Safety* **17**, 47–51.

Gifford, F. A. 1968. An outline of theories of diffusion in the lower layers of the atmosphere. In: *Meteorology and atomic energy*, ed. D. Slade. USAEC TID — 24190, ch. 3. US Atomic Energy Commission, Oak Ridge, Tennessee, USA.

Guicherit, R. and van Dop, H. 1977. Photochemical production of ozone in Western Europe (1971–1975) and its relation to meteorology *Atmos. Environ.* **11**, 145–155.

Hindmarsh, A. C. 1983. ODEPACK, A systematized collection of ODE solvers. In: R. S. Stepleman, ed.: *Numerical methods for scientific computation.* North-Holland, New York, 55–64.

Jeffries, H. E., Sexton, K. G. and Arnold, J. R. 1988. *Validation testing of new mechanisms with outdoor chamber data*, vol. 2. EPA/600/3–89/010c. U. S. EPA Research Triangle Park, North Carolina.

Klug W., Graziani, G., Grippa, G., Pierce, D. and Tassone, C. 1992. *Evaluation of long-range atmospheric transport models using environmental radioactivity data from the Chernobyl accident.* Elsevier Applied Science London and New York, 366 pp.

Lurmann, F. W., Lloyd, A. C. and Atkinson, R. 1986. A chemical mechanism for use in long-range transport/acid deposition computer modelling. *J. Geophys. Res.* **91**, 10905–10936.

MacDonald, A. M., Banic, C. M., Leaitch, W. R. and Puckett, K. J. 1993. Evaluation of the Eulerian acid deposition and oxidants model (ADOM) with summer 1988 aircraft data. *Atmos. Environ.* **27A**, 1019–1034.

McKeen S. A., Hsie, E. Y., Trainer, M., Tallamraju, R. and Liu, S. C. 1991. A regional model study of the ozone budget in the Eastern United States *J. Geophys. Res.* **96**, 10809–10845.

McNaughton D. J., Bowne, N. E., Edgerton, E., Tropp, R., Duffner, K., Londergan, R. and Bryan, J. 1994. Data quality information for the eulerian model evaluation field study surface network, vol. 2: *Analysis of methods suitability, representativeness, network comparability, and data quality.* Electric Power Research Institute Report: TR-102522-V2 Palo Alto, California.

Middleton, P., Stockwell, W. R. and Carter, W. P. 1990. Aggregation and analysis of volatile organic compound emissions for regional modelling. *Atmos. Environ.* **24**, 1107–1133.

Mitchell, H. L., Chouinard, C., Charette, C., Hogue, R. and Lambert, S. J. 1996. Impact of a revised analysis algorithm on an operational data assimilation system. *Mon. Wea. Rev.* **124**, 1243–1255.

Oran, E. S. and Boris, J. P. 1987. *Numerical simulation of reactive flow*. Elsevier Science Publishing New York.

Peterson, J. T. 1976. *Calculated actinic fluxes (290–700 nm) for air pollution photochemistry applications*. US Environmental Protection Agency Report Number: EPA-600/4-76-025.

Pudykiewicz, J. 1989. Simulation of the Chernobyl dispersion with a 3-D hemispheric tracer model. *Tellus* **41B**, 391–412.

Pudykiewicz, J., Benoit R., Mailhot J. 1992. Inclusion and verification of a predictive cloud–water scheme in a regional numerical weather prediction model. *Month. Wea. Rev.* **120**, 612–626.

Robert, A., Yee, T. L. and Ritchie, H. 1985. A semi-Lagrangian and semi-implicit numerical integration scheme for multilevel atmospheric models. *Mon. Wea. Rev.* **113**, 388–394.

Robertson, L. and Persson, C. 1992. On the application of four dimensional data assimilation of air pollution data using the adjoint technique In: *Air pollution modelling and its applications*, ed. H. van Dop. Plenum Press, New York and London, 803 pp.

Seinfeld, J. H. 1986. *Atmospheric chemistry and physics of air pollution*. Wiley, New York, 738 pp.

Simpson, D. 1993. Photochemical model calculations over Europe for two extended summer periods: 1985 and 1989. Model results and comparison with observations. *Atmos. Env.* **27A**, 921–943.

Smolarkiewicz, P. K. and Grell, G. A. 1992. A class of monotone interpolation schemes. *J. Comp. Phys.* **101**, 431–440.

Smolarkiewicz, P. K. and Pudykiewicz, J. A. 1992. A class of semi-Lagrangian approximations for fluids. *J. Atmos. Sci.* **49**, 2082–2096.

Sundqvist, H. 1988. Parameterization of condensation and associated clouds in models for weather prediction and general circulation simulation. In: *Physically-based modeling and simulation of climate and climatic change*, Part I. M. E. Schlesinger, ed. Reidel, Dordrecht, 433–461.

Tanguay, M., Robert, A. and Laprise, R. 1990. A semi-implicit semi-Lagrangian fully compressible regional forecast model. *Mon. Wea. Rev.* **118**, 1970–1980.

U. S. EPA, 1989. The 1985 NAPAP emission inventory (version 2). *Development of the annual data and modelers' tapes*. Rep. EPA-600/7-89-012a, 692 pp Natl. Tech. Info. Serv., Springfield, Va.

Van Dop, H., den Tonkelaar, J. and Briffa, K. R. 1987. A modelling study of atmospheric transport and photochemistry in the mixed layer during anti-cyclonic episodes in Europe. *J. Clim. Appl. Meteorol.* **26**, 1305–1316.

Wesley, M. L. and Hicks, B. B. 1977. Some factors that affect the deposition rates of sulfur dioxide and similar gases on vegetation. *J. Air Pollut. Control Assoc.* **27**, 1110–1116.

Whitten, R. C. and Poppoff, I. G. 1971. *Fundamentals of aeronomy*. John Wiley & Sons, Inc. New York.

Yakimiw, E. and Robert, A. 1990. Validation experiments for a nested grid-point regional forecast model. *Atmos. and Ocean* **28**, 466–472.

Young, T. R. and Boris, J. P. 1977. A numerical technique for solving stiff ordinary differential equations associated with the chemical kinetics of reactive flow problems. *J. Phys. Chem.* **81**, 2424–2427.